



Cite this: *RSC Sustainability*, 2023, 1, 1259

## A pyridinium-modified chitosan-based adsorbent for arsenic removal *via* a coagulation-like methodology†

Deysi J. Venegas-García, Bernd G. K. Steiger and Lee D. Wilson \*

The goal of this study was to synthesize a chitosan-derived adsorbent that can be used in a coagulation–flocculation (CF) process for facile integration into existing water treatment processes. Therefore, an insoluble pyridinium-modified chitosan (Chi-Py) was prepared. Structural characterization was achieved with spectroscopy (FT-IR,  $^{13}\text{C}$  solids NMR, and X-ray photoelectron) methods and thermogravimetric analysis. Approximately 7% di-nitrobenzene and ca. 30% pyridinium moieties were incorporated into the chitosan framework *via* an adapted, moderate-temperature, Zincke reaction. The arsenic removal efficiency was evaluated by a coagulation-inspired methodology at pH 7.5, where the results were compared against CF systems such as pristine chitosan,  $\text{FeCl}_3$  and chitosan– $\text{FeCl}_3$ . The kinetic and van't Hoff thermodynamic parameters for arsenic removal were calculated. Arsenic adsorption was shown to be a spontaneous and exothermic process ( $\Delta G = -4.7 \text{ kJ mol}^{-1}$ ;  $\Delta H = -75.6 \text{ kJ mol}^{-1}$ ) with a 76% arsenic removal efficiency at 23 °C and 96% at 5 °C with a maximum effective adsorbent dosage of Chi-Py of 300 mg L $^{-1}$ . The adsorption process for Chi-Py followed pseudo-first order kinetics, where the pyridinium-modified chitosan adsorbent can be successfully employed similar to coagulant-like systems in conventional water treatment processes. In contrast to conventional adsorbents (1–2 g L $^{-1}$ ), a dosage of only 300 mg L $^{-1}$  was required for Chi-Py that offers greater sustainability and recycling of materials. This is contrasted with single-use conventional coagulants such as  $\text{FeCl}_3$  or binary  $\text{FeCl}_3$ –chitosan CF systems.

Received 28th April 2023

Accepted 19th June 2023

DOI: 10.1039/d3su00130j

rsc.li/rscsus

### Sustainability spotlight

Addressing arsenic water pollution represents a grand environmental challenge due to its widespread occurrence, high mobility and toxicity. Arsenic at elevated groundwater concentrations ("hotspots") occurs across regions of Asia, the Americas, and Europe and represents a key global water security concern to ecosystems and human health. This research uses green chemistry to modify chitosan with suitable properties for dispersed solid phase extraction (dsPE) that reveals unique advantages over other conventional adsorbents. The facile and low-cost approach described herein is suitable for scale-up and implementation in current water treatment technologies for the sustainable treatment of arsenic-laden groundwater. Our work emphasizes the importance of the following UN sustainable development goals: water and sanitation (SDG 6); industry, innovation and infrastructure (SDG 9).

## 1. Introduction

Arsenic is a highly toxic pollutant prevalent in aqueous sources such as ground water, soils and sediments. Arsenic release into the environment can occur through natural processes (erosion and leaching) or anthropogenic activities (mining, pesticides).<sup>1</sup> Through various physical processes, water soluble arsenate species can be ingested upon dissolution, which results in detrimental effects on the ecosystem and human health.

Arsenic exists in variable oxidation states and chemical forms such as organoarsenicals (monomethylarsonate, dimethylarsinate, roxarsone) or as inorganic oxyanions (As(III) or As(V)).<sup>2,3</sup> The latter pose a significant risk for human health through tainted water sources, hence; drinking water advisories (e.g., Canada, WHO) have set limits to arsenic levels at 10 µg L $^{-1}$ .<sup>4,5</sup> Mine tailings and various anthropogenic activities may result in greater arsenic levels, as highlighted by a comparative study with elevated levels of arsenic (0.7–5.5 mg L $^{-1}$ ) in specific surface waters for lakes near Yellowknife.<sup>6,7</sup> Such arsenic concentrations exceed the regulatory limits and require cost-effective techniques that can be readily integrated into conventional water treatment processes. In aqueous media atoxic conditions, As(V) is the dominant species at environmentally relevant conditions, where a near 1 : 1 mixture of  $\text{H}_2\text{AsO}_4^-$

Department of Chemistry, University of Saskatchewan, 110 Science Place – Room 156 Thorvaldson Building, Saskatoon, SK S7N 5C9, Canada. E-mail: lee.wilson@usask.ca; Tel: +1-306-966-2961

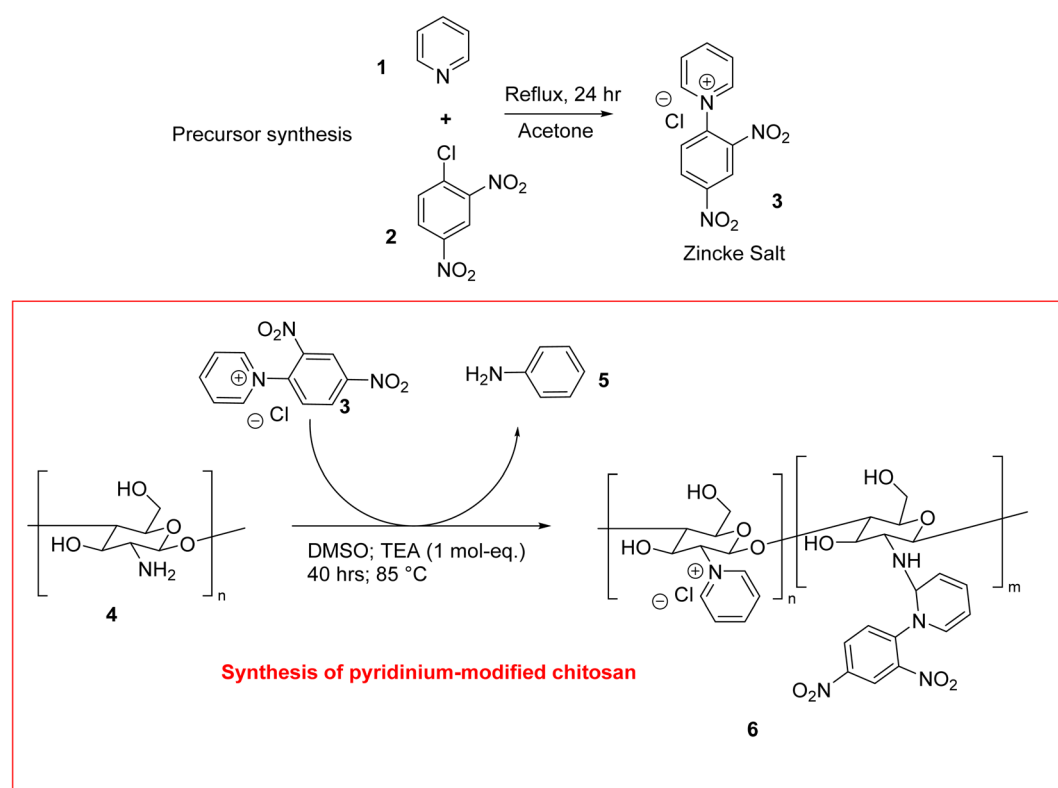
† Electronic supplementary information (ESI) available: Table S1: Effect of temperature on arsenic removal evaluated through kinetic experiments for Chi-Py. See DOI: <https://doi.org/10.1039/d3su00130j>



and  $\text{HAsO}_4^{2-}$  co-exist at pH 7.<sup>8,9</sup> Various remediation techniques such as precipitation, membrane filtration, reverse osmosis and adsorption are known that display variable arsenic removal efficiency.<sup>10–12</sup> While efficient removal is desired, access to low-cost and low-maintenance methods can increase the viability of effective and sustainable water treatment. Adsorption-based processes meet such criteria, especially when employing biopolymer adsorbents.<sup>13–16</sup> Globally, water treatment plants (WTPs) employ either coagulation or coagulation-flocculation (CF) processes for contaminant removal, where the selection of the coagulants and flocculants is of paramount importance to facilitate effective contaminant removal. Biopolymers have several advantages such as affordability, relative abundance, as exemplified by sustainable materials like cellulose-based CF systems.<sup>17</sup> Recent research efforts have been directed at development of alternate polysaccharide-based CF systems such as chitosan (Chi).<sup>18</sup> Chi represents a promising and versatile biopolymer that is derived from chitin, the second most abundant natural biopolymer.<sup>19–21</sup> Chitosan is a partially deacetylated form (typically >50%) of chitin, which has hydroxyl and amine groups that present additional functionalization sites. A study by Billah *et al.* highlighted a modified chitosan-based adsorbent with  $12.32 \text{ mg g}^{-1}$  adsorption capacity at pH 5 with 99% removal.<sup>22</sup> However, arsenic removal studies *via* chitosan-based adsorbents are limited by its  $\text{p}K_a$  (*ca.* 6.5), where chitosan's arsenic removal efficacy drastically decreases at pH >

6,<sup>23–27</sup> where acidic conditions ( $\text{pH} < 6$ ) are required for optimum uptake.<sup>21</sup> However, this is in contrast with the regularly encountered pH of natural water sources such as ground water with slightly alkaline pH conditions (*ca.* pH 7–8).<sup>26</sup> Optimal chitosan-based adsorbents should be designed to obviate pH adjustments to afford more efficient water treatment. One such example for removal at pH 7 can be found in chitosan-loaded MgAl layered double hydroxides.<sup>28</sup> The amine groups of chitosan are amenable to chemical modification to yield cationic functional groups. One such example was reported by Chen *et al.*, where a pyridinium-moiety was grafted onto the amine-group of chitosan *via* a linker unit.<sup>29</sup> However, a more direct approach is the conversion of the amine group into a pyridinium chloride moiety, according to the well-known Zincke reaction, which has been utilized to obtain such chitosan derivatives.<sup>30,31</sup> The Zincke reaction is envisaged to require a lower temperature and shortening of the reaction time to yield a cationic form with variable hydration properties *via* a lower energy synthesis (*cf.* Scheme 1).<sup>32,33</sup> The pyridinium-modified chitosan is posited to function as an adsorbent for efficient arsenic removal due to the pyridyl grafted units and its reduced hydrophile character (*versus* chitosan), where such differences in biopolymer hydration are likely to enhance arsenate uptake *versus* sulfate or nitrate oxyanions.<sup>34</sup>

Water treatment plants currently employ coagulation-flocculation (CF) processes on a wide scale, especially where



**Scheme 1** Schematic overview of the synthesis of chitosan–pyridinium (6) based on the reaction of the Zincke salt precursor, *N*-(2,4-benzene) pyridinium chloride (3), along with subsequent conversion of chitosan (4) under aniline (5) formation in dimethyl sulfoxide (DMSO) as solvent and triethylamine (TEA) as an additional base.



inorganic coagulants such as alum and ferric salts are utilised with or without flocculants. A key feature of efficient CF-based water treatment relies on floc formation to enable phase separation of contaminants from treated water. Currently, a drawback of conventional chemical systems is the lack of biodegradability, which as been described elsewhere.<sup>18</sup> Whereas the co-application of biodegradable polymers or biopolymers such as plant-based mucilage in conjunction with metal-salt coagulants offer an alternative strategy. Herein, a modified chitosan-based system was utilized as a dispersed solid-phase extraction (dSPE) material, where the insoluble adsorbent was directly added to afford facile separation during the treatment process.<sup>35</sup>

The key feature of this study is the facile integration of an adsorbent material into an existing process without the need to employ high dosages common to classical adsorption or extraction processes.<sup>36–38</sup> Hence, it is posited that modified Chi can facilitate the transition from non-biodegradable materials to more sustainable water treatment options, whilst obviating the need for pH adjustments of the wastewater system. Furthermore, this facile integration into coagulation–flocculation processes negates the need to increase pH for dosage-dependent removal efficiency as for the use of iron(III) salts.<sup>39–42</sup>

This work will contribute to the field of sustainable water treatment for removal of arsenic species in aqueous media at neutral pH conditions by employing a natural biopolymer (chitosan) that typically requires more acidic conditions to be feasible.

## 2. Materials and methods

### 2.1. Materials

**2.1.1 Chemicals.** All chemicals were of analytical reagent (ACS) grade unless otherwise stated. Ferric chloride hexahydrate (97%), sodium hydroxide (99%), hydrochloric acid (35%), potassium antimony(III) tartrate hydrate (99%), antimony molybdate tetrahydrate (99.9%) and potassium bromide (FT-IR grade, 99%) were purchased from Sigma-Aldrich (Oakville, ON, CA). Sodium hydrogen arsenate heptahydrate (98%) was obtained from Alfa Aesar (Tewksbury, MA, USA). Chitosan (Low molecular weight, DDA *ca.* 80%), 1-chloro-2,4-dinitrobenzene, pyridine (99.8%) and *N,N*-dimethylformamide (HPLC grade, DMF) were acquired from Sigma-Aldrich (Oakville, Canada). Dimethyl sulfoxide (DMSO) and toluene were procured from BDH (West Chester, USA). Ethanol was purchased from Greenfield Global (Brampton, Canada). Triethyl amine (TEA) was obtained from (EMD, Darmstadt, Germany). L-Ascorbic acid (99%) was obtained from BDH Chemicals (Mississauga, ON, Canada). All materials were used as received unless specified otherwise. All stock solutions were prepared using 18 MΩ cm Millipore water.

**2.1.2 Synthesis of *N*-(2,4-dinitrophenyl) pyridinium chloride (Zincke salt).** 3.66 g (17.5 mmol, 1 eq.) of 1-chloro-2,4-dinitrobenzene were added to a solution of 1.43 mL (17.7 mmol, 1.1 eq.) in 17 mL acetone under stirring. The solution was refluxed under stirring for 24 h. The white precipitate (80% yield) was washed with acetone and filtered.

**2.1.3 Synthesis of pyridinium-modified chitosan (Chi-Py).** 1.32 g (0.0047 mol, 3 eq.) Zincke salt was dissolved in 21 mL DMSO and 0.25 g chitosan (0.00155 mol, 1 eq.; based on glucosamine monomers assuming 100% deacetylation) was added while stirring. Then, 0.218 mL (0.00155 mol, 1 eq.) of TEA was added and the mixture was stirred *ca.* 85 °C for 40 h. Afterwards, *ca.* 20–60 mL DMSO was added, followed by gravity filtration (Whatman filter paper 202) of the mixture, along with sequential solvent washing of the filtrate with *ca.* 50 mL DMSO, *ca.* 50 mL toluene, *ca.* 100 mL dimethyl formamide (DMF) until solvent had a clear appearance without coloration after passing through the filter. A final washing with ethanol (50 mL) was followed by air-drying overnight at *ca.* 22 °C.

### 2.2. Characterization

**2.2.1 <sup>13</sup>C solids NMR spectroscopy.** <sup>13</sup>C solids NMR spectra were obtained with a 4 mm DOTY CP-MAS probe and a Bruker AVANCE III HD spectrometer operating at 125.77 MHz (<sup>1</sup>H frequency at 500.13 MHz). The <sup>13</sup>C CP/TOSS (cross polarization with total suppression of spinning sidebands) spectra were obtained at a sample spinning speed of 7.5 kHz, a <sup>1</sup>H 90° pulse of 5  $\mu$ s, and a contact time of 2.0 ms, with a ramp pulse on the <sup>1</sup>H channel. Spectral acquisition required *ca.* 2500 scans with a 1 s recycle delay, along with a 50 kHz SPINAL-64 decoupling sequence. <sup>13</sup>C NMR chemical shifts were externally referenced to adamantane at 38.48 ppm (low field signal).

**2.2.2 FT-IR spectroscopy.** The FT-IR spectra were recorded using a Bio-Rad FTS-40 (Bio-Rad Laboratories, Inc., USA) in reflectance mode, where dry samples were co-ground and mixed *via* mortar and pestle with FT-IR grade KBr in a 1 : 10 weight ratio (sample : KBr). The diffuse reflectance infrared Fourier transform (DRIFT) spectra were obtained at 295 K over a spectral range of 400–4000 cm<sup>−1</sup> with a resolution of 4 cm<sup>−1</sup>, where a minimum of 128 scans were recorded and corrected relative to a background spectrum of KBr.

**2.2.3 Thermogravimetric analysis (TGA).** The weight loss profiles were obtained using a Q50 TA Instruments thermogravimetric analyzer (TA Instruments, USA). Samples were heated in open aluminium pans at 30 °C for 5 min to allow for equilibration prior to heating at 5 °C min<sup>−1</sup> to 500 °C.

**2.2.4 X-ray photoelectron spectroscopy (XPS).** All X-ray Photoelectron Spectroscopy (XPS) measurements were collected using a Kratos (Manchester, UK) AXIS Supra system at the Saskatchewan Structural Sciences Centre (SSSC) under UHV conditions. This system is equipped with a 500 mm Rowland circle monochromated Al K- $\alpha$  (1486.6 eV) source and combined hemi-spherical analyzer (HSA) and spherical mirror analyzer (SMA). A spot size of 300 × 700 microns was used. All survey scan spectra were collected in the −5 to 1200 binding energy range in 1 eV steps with a pass energy of 160 eV. High resolution scans of 4 regions were also conducted using 0.1 eV steps with a pass energy of 20 eV. An accelerating voltage of 15 keV and an emission current of 10 mA were used for the analysis. Data processing was done with CasaXPS.<sup>43</sup> The spectra were calibrated against adventitious carbon at 284.8 eV.



### 2.3. Arsenic removal methods

**2.3.1 Arsenic adsorption process.** The adsorption experiments were tested following a coagulation-like methodology using a program-controlled conventional jar test Phipps & Bird PB-900 apparatus (Richmond, VA, USA) with six 2 L jars and stirrers. The system studied was arsenic with an initial concentration of  $5 \text{ mg L}^{-1}$ . Approximately 1 L of simulated arsenic-containing sample was added to the jar tester vessel and the pH was adjusted using 0.1 M NaOH or 0.1 M HCl to 7.5  $\pm$  0.4. An aliquot of the arsenic solution was sampled to measure initial arsenic concentration. A predetermined amount of material was added to the solution, followed by rapid stirring for 3 min at 295 rpm. Thereafter, the stirring rate was reduced to 25 rpm for 20 min. Then, the stirring was stopped and the solutions were allowed to settle for 90 min. Then, a 3 mL sample was used for UV-vis spectral analysis by adding 0.5 mL of molybdate reagent, as described elsewhere (limit of detection *ca.*  $5 \mu\text{g L}^{-1} \pm 5 \mu\text{g L}^{-1}$ ).<sup>44,45</sup> After addition of the reagent to the arsenic sample, a blue colored complex formed after 20 min before the UV-vis absorbance values were recorded. A calibration curve of arsenic was obtained using the molybdate colorimetric method ( $\lambda = 900 \text{ nm}$ ) using a SPECTRONIC 200 Visible Spectrophotometer (Waltham, MA, USA). Experiments were repeated in a duplicate manner, and the average value was reported. The removal efficiency (RE; %) of arsenic and the adsorption capacity,  $q_e$  (arsenic;  $\text{mg g}^{-1}$ ) were calculated by eqn (1) and (2), respectively.

$$\text{RE}(\%) = \frac{C_o - C_e}{C_o} \times 100 \quad (1)$$

$$q_e = \frac{(C_o - C_e) \times V}{m} \quad (2)$$

Here,  $C_o$  and  $C_e$  are the initial and equilibrium concentrations ( $\text{mg L}^{-1}$ ) of arsenic,  $V$  is the volume (L), and  $m$  is the total weight (g) of the system (flocculant).

**2.3.2 Kinetic studies.** The kinetics of the arsenic removal were investigated through the Pseudo-First Order (PFO; eqn (3)) and Pseudo-Second Order (PSO; eqn (4)) kinetic models as described below:

$$q_t = q_e(1 - e^{-k_1 t}) \quad (3)$$

$$q_t = \frac{q_e^2 k_2 t}{1 + q_e k_2 t} \quad (4)$$

$q_t$  ( $\text{mg g}^{-1}$ ) and  $q_e$  ( $\text{mg g}^{-1}$ ) hereby indicate the adsorption capacity at time ( $t$ ) and equilibrium respectively.  $k_1$  ( $\text{min}^{-1}$ ) and  $k_2$  represent the respective rate constants for these kinetic models.

Kinetic studies were performed *in situ* using a one-pot method (Fig. 1), as described by Venegas-García & Wilson.<sup>46</sup> Briefly, a 600 mL beaker containing 400 mL of 5 mg per L arsenic solution (pH 7.5) was mixed by magnetic stirring. A filter paper (Whatman no. 40) was folded into a cone and attached to the beaker that was immersed in the solution at a depth of 2 cm whilst stirring at a fixed rate (25 rpm). An initial 3 mL was sampled from within the filter cone interior. Sampling within the filter cone began at time ( $t = 0$ ), when the coagulant-based material was added, which continued at 1 min intervals for 10 min, then for a further 10 min at 2 min intervals, and finally for 50 min at 5 min intervals. Stirring was stopped at  $t = 30$  min. After 50 min, sampling continued for a further 40 min at 10 min intervals. Sample aliquots were prepared for UV-vis spectral analysis, as discussed above. The adsorption capacity at different times was determined using eqn (2). To measure adsorption kinetics at variable temperatures, the one-pot

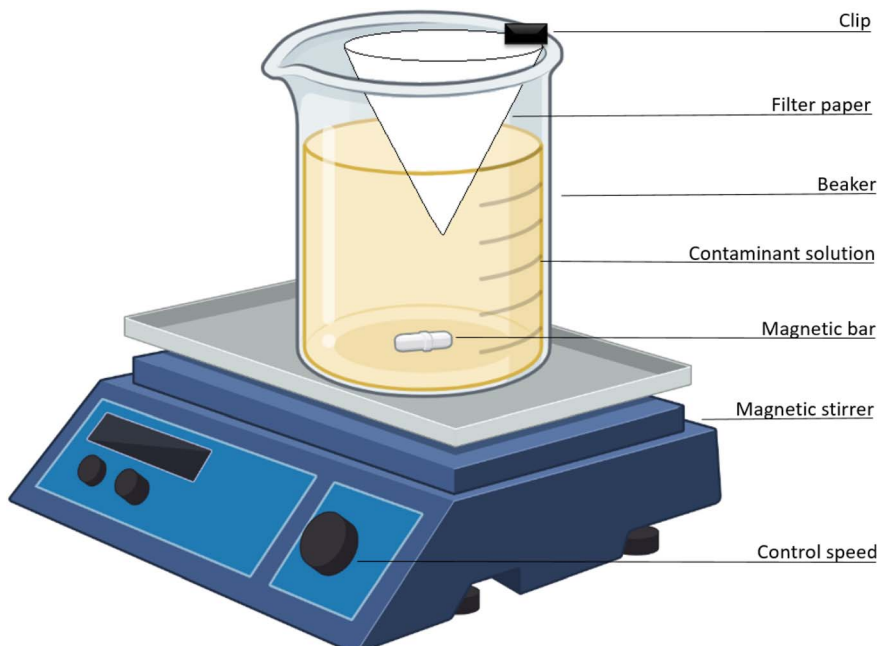


Fig. 1 Illustration of the one-pot method for *in situ* kinetic adsorption studies.



experiment was thermally regulated using an Endocal refrigerated circulating bath (−40 to 40 °C) with flow control (Neslab, Newington, NH, USA) at 23 °C, 15 °C, and 5 °C ± 0.5 °C.

**2.3.3 Thermodynamic studies.** To describe whether the process is endothermic or exothermic, isotherms were obtained at several different temperatures to derive the standard difference in the thermodynamic parameters:  $\Delta G^\circ$ ,  $\Delta H^\circ$  and  $\Delta S^\circ$ , where the interrelationship of these parameters is expressed by eqn (5):

$$\Delta G^\circ = \Delta H^\circ - T\Delta S^\circ \quad (5)$$

To obtain  $\Delta G^\circ$  for calculation of  $\Delta H^\circ$  and  $\Delta S^\circ$ , eqn (6) and (7) were used:

$$\Delta G^\circ = -RT \ln K_e \quad (6)$$

$$\ln K_e = -\left(\frac{\Delta H^\circ}{RT}\right) + \left(\frac{\Delta S^\circ}{R}\right) \quad (7)$$

$K_e$  is described as the thermodynamic equilibrium constant ( $K_e$ ; L g<sup>−1</sup>) for a liquid/solution partitioning process (where  $K_e = q_e/C_e$ ), and  $q_e$  (mg g<sup>−1</sup>) refers to the equilibrium quantity of the adsorbed adsorbate. The adsorbate concentration at equilibrium is referred to as  $C_e$  (mg L<sup>−1</sup>).  $R$  is the universal gas constant (8.3145 J K<sup>−1</sup> mol<sup>−1</sup>) and  $T$  is the temperature in Kelvin (K).

To obtain the thermodynamic parameters, the slope of a plot of  $\ln K_e$  vs.  $1/T$  (slope =  $-\Delta H^\circ/R$ ; intercept =  $\Delta S^\circ/R$ ) was obtained.

### 3. Results and discussion

The following section is divided into three parts, where the first part covers the structural characterization of the material. The second section characterizes the utility of Chi-Py for the removal of arsenic *via* the CF-methodology, where the results are compared against single component systems (chitosan or FeCl<sub>3</sub>) or a binary system (Fe-chitosan) at pH 7.5. The third part

describes the kinetic and thermodynamic parameters of arsenic adsorption onto Chi-Py to evaluate the adsorptive removal at variable temperatures.

#### 3.1. Characterization

**3.1.1 <sup>13</sup>C solids NMR spectroscopy.** <sup>13</sup>C solids NMR spectra were used to identify whether the biopolymer backbone structure of chitosan was successfully modified, and the pyridinium moieties incorporated (Fig. 2).

Herein, the characteristic polysaccharide backbone was visible between 110 and 50 ppm for chitosan, with additional signals at 23 ppm (acetyl-CH<sub>3</sub>) and 173 ppm (acetyl-C=O).<sup>47</sup> The pyridinium-modified chitosan also observes these signals, but also has three broad overlapping signals between 165 and 120 ppm in addition, indicating additional aromatic moieties stemming from partially converted, attached *N*-2,4-dinitrobenzene (around 160 ppm).<sup>48,49</sup> In addition, a sharp signal at 18 ppm appeared, which could indicate *N*-2,4-dinitrobenzene-groups adjacent to the acetyl-moiety, as the reactants observe different shifts in ppm, where triethyl ammonium chloride occurs near 10 and 46 ppm.<sup>50</sup>

**3.1.2 IR spectroscopy.** IR spectroscopy can be used to identify functional groups within materials, where the FT-IR spectra of the unmodified chitosan and pyridinium-modified chitosan are shown in Fig. 3.

For chitosan, the band around 3500 cm<sup>−1</sup> can be ascribed to its −NH and −OH groups, whereas the −CH bands can be observed near 2800 cm<sup>−1</sup>. The amine-groups of chitosan concur with the band at 1661 cm<sup>−1</sup> (amide C=O), in conjunction with 1163 cm<sup>−1</sup> and 1123 cm<sup>−1</sup>, which are identified as C–O and C–H stretching.<sup>20</sup> A small signature around 2095 cm<sup>−1</sup> relates to −CH stretching. For pyridinium-modified chitosan, these IR signals appear abated and additional bands between 3500 and 2250 cm<sup>−1</sup> are visible, which are attributed to aromatic CH bands.<sup>48,49</sup> Furthermore, a strong band at 1657 cm<sup>−1</sup> can be ascribed to a conjugated C=N band. The broad and strong IR

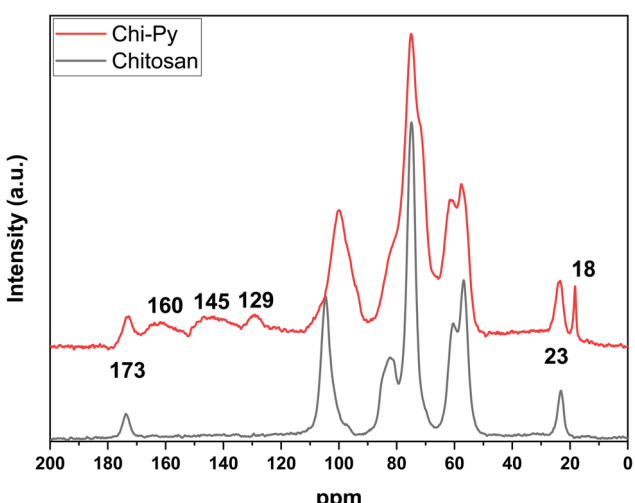


Fig. 2 <sup>13</sup>C CP-TOSS solids NMR spectra of chitosan and the pyridinium-modified chitosan.

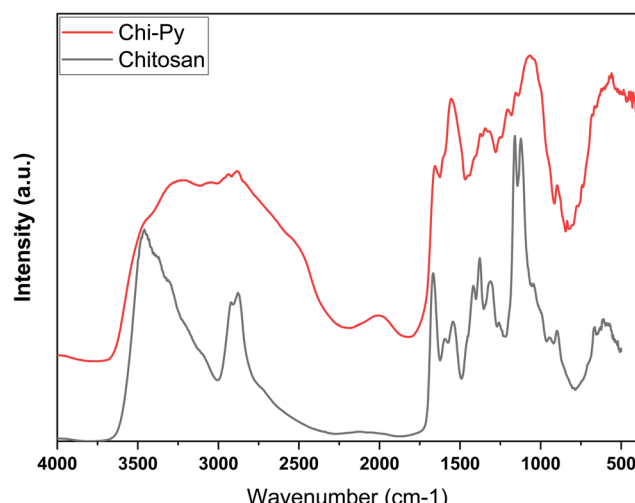


Fig. 3 FT-IR spectra of the precursor chitosan and the pyridinium-modified chitosan.



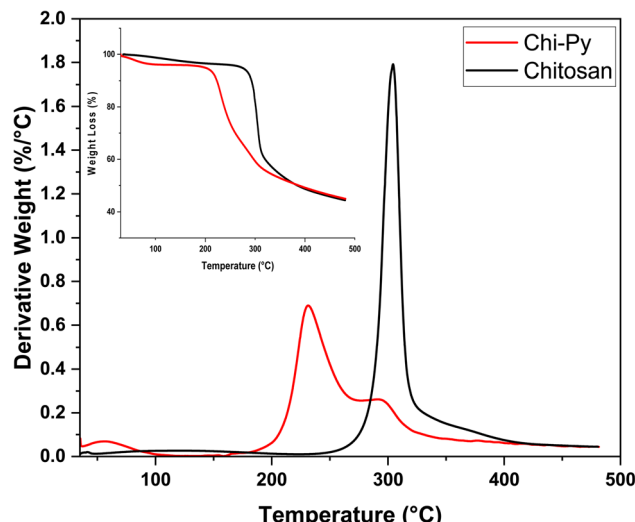


Fig. 4 TG (inset) and DTG profiles of chitosan and Chi-Py.

band near  $1545\text{ cm}^{-1}$  concurs with  $\text{C}=\text{C}$  (aromatic) contributions.<sup>51,52</sup>

**3.1.3 Thermogravimetric analysis.** Thermogravimetric (TG) and derivative TG (DTG) profiles can reveal the role of chemical modifications and the thermal stability of materials (*cf.* Fig. 4).

In the DTG profile, a greater water loss centred near  $50\text{ }^\circ\text{C}$  is noted for Chi-Py, as compared to pristine chitosan.<sup>53,54</sup> Chitosan is characterized by a sharp peak (onset *ca.*  $250\text{ }^\circ\text{C}$ , maximum  $305\text{ }^\circ\text{C}$ ), which can be assigned to the dehydration, depolymerization and decomposition of *N*-acetyl- and amine groups.<sup>55</sup> Chi-Py, on the other hand, shows a large decomposition event shifted to a lower temperature onset (*ca.*  $170\text{ }^\circ\text{C}$ ) with a maxima near  $230\text{ }^\circ\text{C}$ , which coincides with a second, smaller decomposition event with a maxima near  $290\text{ }^\circ\text{C}$ , which can be ascribed to the chitosan backbone. It is posited that the pyridinium-moiety induces this shift in stability to lower

temperatures, due to disruption of the semi-crystalline structure of unmodified chitosan. Parallel trends have been ascribed to modified cellulosic materials, which is related to disruption of the interchain hydrogen bonding of cellulose.<sup>56,57</sup> Additionally, the TG profiles (*cf.* inset in Fig. 4) show a similar remaining weight at  $500\text{ }^\circ\text{C}$ , indicating that the carbonized backbone remains, which displays similar trends for both biopolymers.

**3.1.4 X-ray photoelectron spectroscopy (XPS).** Herein, XPS was used to corroborate the FT-IR and NMR spectral results, which includes an analysis of the Chi-Py material in the pre- and post-states of the arsenic adsorption process. In particular, XPS provided elemental quantification and oxidation state of the N-atoms, as illustrated in Fig. 5 and Table 1.

Based on the survey scan of Chi-Py before and after adsorption (Chi-Py As(v)), elemental quantification was performed to support that arsenic is adsorbed onto the insoluble Chi-Py derivative and to investigate whether the chloride content decreased (*cf.* Table 1).

In the pristine material, chloride was present and was quantified to *ca.* 3.6 wt%. As expected, arsenic could not be identified in the pristine material before adsorption. After adsorption, a small amount of arsenic (0.81 wt%) was quantified in the matrix of Chi-Py, with a slightly lower average chloride content (3.2 wt%). This trend indicates anion exchange as adsorption mechanism and coordination of arsenic while replacing chloride.

In addition, the N 1s narrow scan was performed to elucidate the oxidation states of nitrogen within the material before and after adsorption (*cf.* Fig. 6) using a binding energy window wide enough to capture all possible nitrogen species.<sup>58</sup>

The peak around  $399.50\text{ eV}$  in Chi-Py and  $399.78\text{ eV}$  in Chi-Py As(v) was identified as the amine band, whereas the pyridinium signature appeared at  $402.03\text{ eV}$  and  $402.20\text{ eV}$  in Chi-Py and Chi-Py As(v), respectively. The identified nitro-group nitrogen appeared at  $495.95\text{ eV}$  in Chi-Py and  $406.07\text{ eV}$  in Chi-Py As(v) respectively.<sup>59</sup> While inhomogeneities and variable surface characteristics alter the local elemental concentrations, which results in variable elemental quantification. For example, the N-atom of the nitro-group was quantified as 14.49 atom% in Fig. 6A and 14.24 atom% in Fig. 6B. Based on this evaluation, it can be concluded that after exposure to aqueous media, negligible levels of di-nitro compound dissolved and remained bound to the material. The stability of Chi-Py does not pose

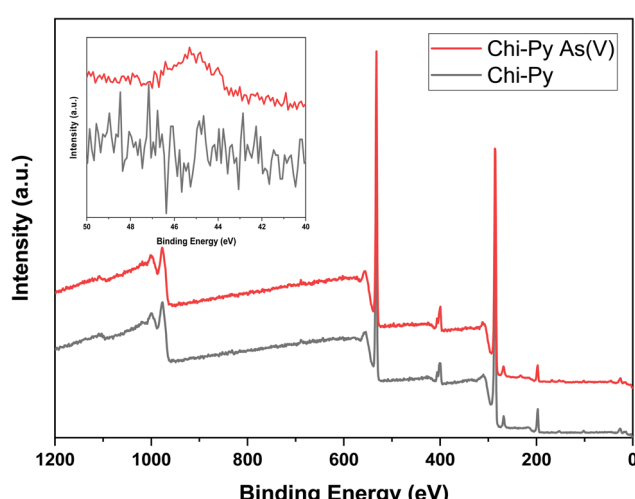


Fig. 5 XPS survey scan of Chi-Py before (Chi-Py) and after arsenic adsorption (Chi-Py As(v)) with the As 3d narrow scan as the inset.

Table 1 Weight% of the two measured spots on Chi-Py (including average)

	Chi-Py			Chi-Py As(v)		
	Spot 1	Spot 2	Average	Spot 1	Spot 2	Average
C	62.27	60.32	61.30	61.68	63.03	62.36
N	5.93	6.97	6.45	5.93	5.62	5.78
O	26.85	26.81	26.83	27.58	28.18	27.88
Cl	4.95	2.26	3.61	3.44	2.95	3.20
As	0	0	0	1.39	0.22	0.81



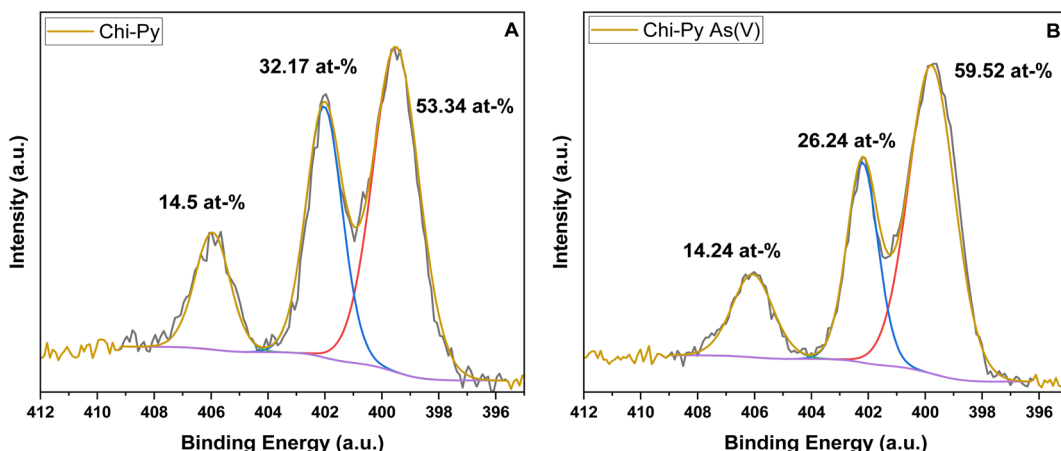


Fig. 6 The oxidation state of nitrogen via N 1s narrow scan of the pristine Chi-Py (A) and Chi-Py As(V) after (B) adsorption.

significant risks to aquatic life due to its chemical stability and relative insolubility in aqueous media.

### 3.2. Arsenic removal *via* a coagulation-like methodology

**3.2.1 Removal experiments.** This study was focused on the synthesis and application of chitosan-based coagulant for the removal of As(v) in water. Estimates of the  $\zeta$ -potential by Guo *et al.* reveal that Chi-Py is positively charged at pH < 8.6. It is well known that the removal of arsenic depends on several factors (coagulant dosage, initial pH, settling time, initial arsenic concentration). Some of these factors concur with reports in the literature for arsenic removal that employ coagulation-flocculation (CF) processes. Coagulant dosages from 1 to 400 mg L<sup>-1</sup> were evaluated, as shown in Fig. 7 and Table 2, where the arsenic removal increases dramatically as the Chi-Py dosage increases from 1 to 150 mg L<sup>-1</sup> (from 0 to ~70% removal). At dosage values of 150 mg L<sup>-1</sup> of Chi-Py, the removal of arsenic

increases only slightly, where a constant arsenic concentration is achieved (~76% removal) from 300 to 400 mg L<sup>-1</sup>.

The removal (%) of arsenic through chitosan (single component system) and a binary system (Fe-chitosan) was investigated under the same conditions at pH 7.5 and 23 °C (*cf.* Table 2) until a decrease in the removal efficiency was observed.

Under same conditions for arsenic concentration and pH, pristine chitosan, FeCl<sub>3</sub> and Fe-chitosan were tested as CF systems to compare with the efficiency of Chi-Py. Pristine chitosan as the coagulant for arsenic removal under an initial pH 7.5, showed a low efficiency of removal (4%, see Table 2). This can be attributed to greater chitosan solubility (at acidic pH) and surface charge (pH<sub>pzc</sub> = 6.5), especially for pH < pH<sub>pzc</sub>. Application of FeCl<sub>3</sub> as coagulant showed a 73% removal almost comparable with the Chi-Py material (76%). Finally, for the process with FeCl<sub>3</sub> as coagulant and pristine chitosan as the flocculant, a 69% removal efficiency was reached. Additional comparison of arsenic removal through various coagulants and flocculants was outlined in Table 3, where a comparison of the results for the Chi-Py obtained herein with other biopolymer systems reveal that comparable arsenic removal (%) could be achieved.

### 3.3. Kinetic and thermodynamic investigation of Chi-Py

After evaluation of the arsenic removal efficacy of Chi-Py with the jar test apparatus, an investigation of the kinetics and thermodynamic parameters of the arsenic removal by Chi-Py were estimated by employing an analogous experimental approach *via* a one-pot setup (*cf.* Fig. 1). The one pot setup enables *in situ* sampling and further insight on the arsenic adsorption process, along with the capability of adsorption kinetics at variable temperature conditions.

**3.3.1 Kinetics.** Table 4 lists the kinetic parameters, where a high correlation was found with the PFO model, which infers the concentration dependence of one component (arsenic) for the removal kinetics. The higher  $R^2$  value of the PFO model was compared to the PSO model, which indicates that the process follows first order kinetics. The relatively low  $R^2$  value (<0.95)

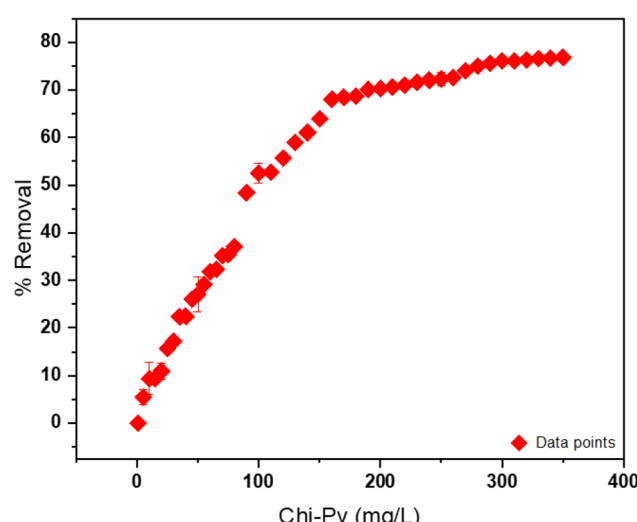


Fig. 7 Removal% and Chi-Py dosage evaluation from 1–400 mg L<sup>-1</sup> with constant arsenic(v) concentration at 23 °C and pH 7.5.



**Table 2** Arsenic % removal of chitosan as single component, iron(III) chloride as a single component, and (Fe–chitosan) with iron(III) chloride for a binary system at pH 7.5 and 23 °C

EXP	Single component		Single component		Binary system		
	Chitosan (mg L <sup>-1</sup> )	% removal	Fe <sup>3+</sup> (mg L <sup>-1</sup> )	% removal	Fe <sup>3+</sup> (mg L <sup>-1</sup> )	Chitosan (mg L <sup>-1</sup> )	% removal
1	0.5	1.6	8.3	3.2	8.3	5	4.1
2	1.0	2.4	7.1	5.7	7.1	5	4.1
3	3.0	3.2	6.3	8.9	6.3	5	4.9
4	5.0	4.1	5.6	73.9	5.6	5	4.9
5	10.0	1.6	5	68.1	5	5	57.2
6	20.0	1.6	4.6	58.9	4.6	5	69.1
7	50.0	1.6	4.2	53.9	4.2	5	63.5
8	100.0	1.6	3.8	46	3.9	5	43.7

obtained herein may be the result of employing a water insoluble adsorbent in a one-pot coagulation experiment, as described by Venegas-García & Wilson.<sup>46</sup> The approach illustrated in Fig. 1 is compared to a conventional kinetic setup with constant stirring that employs a filter barrier, as described by Mohamed *et al.*<sup>60</sup>

The adsorption process of arsenic occurs into two stages: a fast initial adsorption process, where *ca.* 90% of the equilibrium adsorption capacity was reached, followed by a subsequent slow adsorption process, where the adsorption capacity gradually approaches pseudo-equilibrium conditions. The kinetic behavior of Chi-Py for the removal of arsenic is shown in Fig. 8, where the two kinetic models (PFO and PSO) were used to fit the kinetic adsorption profiles for the removal of As(v).

The better fit for the PFO kinetic model mirrors the trends observed for the removal of other pollutants during the CF process, unlike classical adsorption processes, as outlined elsewhere.<sup>18,46,61</sup> This further highlights the applicability of the prepared material for arsenic removal through this one-pot process, as compared to (batch) adsorption removal.

To study the effect of temperature on the kinetics for the removal of arsenic, variable temperature conditions were tested. Fig. 9 shows that the kinetics for arsenic removal at 5, 15, and 23 °C. Kinetic results for arsenic showed that by increasing the temperature from 5 to 23 °C, the adsorption capacity decreased from 8.9 to 7.0 mg g<sup>-1</sup>. Temperature is a crucial parameter in adsorption processes, where the adsorption-

desorption equilibrium can be shifted by an increase or decrease in temperature. For example, exothermic adsorption processes may observe increased desorption upon increased temperatures.<sup>62</sup>

**3.3.2 Adsorption thermodynamics.** To gain insight into the adsorption process, thermodynamic parameters were estimated by a van't Hoff analysis of isotherm results at variable temperature. To attain the parameter of the arsenic adsorption onto Chi-Py, the temperature was varied from 5 to 23 °C. The thermodynamic parameters such as the standard difference in Gibbs energy ( $\Delta G^\circ$ ), enthalpy change ( $\Delta H^\circ$ ), and entropy change ( $\Delta S^\circ$ ) were subsequently determined from the temperature dependence of the equilibrium adsorption constant, as illustrated in Fig. 10.

Table 5 shows the thermodynamic parameters:  $\Delta G^\circ$ ,  $\Delta H^\circ$ , and  $\Delta S^\circ$ . The negative value of  $\Delta G^\circ$  indicates the spontaneity of the process and shows that the adsorption is favourable for arsenic, which proceeds less favourably as the temperature increases with an accompanying decrease in  $q_e$ . Negative values of the Gibbs free energy ( $\Delta G^\circ$ ) with greater magnitude indicates a greater driving force for the adsorption. Negative values for the change in enthalpy ( $\Delta H^\circ$ ) confirmed that the process is exothermic in nature, which supports that the process is physical adsorption, and provides the main driving force that governs the  $\Delta G^\circ$  for the process. According to Ohale *et al.*<sup>63</sup> an adsorptive process is physical in nature if the values of  $\Delta H <$

**Table 3** A comparison of maximum % removal of arsenic in aqueous media using different coagulation–flocculation systems adapted from a previous report by Venegas-García & Wilson<sup>18,a</sup>

Flocculant (mg L <sup>-1</sup> )	Concentration (mg L <sup>-1</sup> )	Coagulant	Concentration (mg L <sup>-1</sup> )	As(v) (mg L <sup>-1</sup> )	pH	Removal (%)
Aloe vera gum	2	PAC	3	0.2–1	5	92.6
Chitosan	0.5	FeCl <sub>3</sub>	—	0.2–1	7	<i>ca.</i> 100
<i>Opuntia ficus-indica</i> gum	350	—	—	0.002–0.01	5.9	70
—	—	FeCl <sub>3</sub>	27.029	1	5	98
—	—	Fe <sub>2</sub> (SO <sub>4</sub> ) <sub>3</sub>	100	5	6	99
—	—	Al <sub>2</sub> (SO <sub>4</sub> ) <sub>3</sub>	25–50	0.065–0.216	7–8	81
Flaxseed gum	64	FeCl <sub>3</sub>	35	50	7	90
Fenugreek gum	52	FeCl <sub>3</sub>	33	50	7	90

<sup>a</sup> Adapted from Table 4 in ref. 18.

Table 4 Kinetic adsorption parameters for Chi-Py coagulation-like process for arsenic at pH 7.5 and 23 °C

Pseudo-first order model			Pseudo-second order model		
$k_1$ (min <sup>-1</sup> )	$q_e$ (mg g <sup>-1</sup> )	$R^2$	$k_2$ (M <sup>-1</sup> min <sup>-1</sup> )	$q_e$ (mg g <sup>-1</sup> )	$R^2$
$0.0609 \pm 0.008$	$2.9739 \pm 0.1481$	0.912	$0.0060 \pm 0.0019$	$9.3635 \pm 0.8040$	0.880

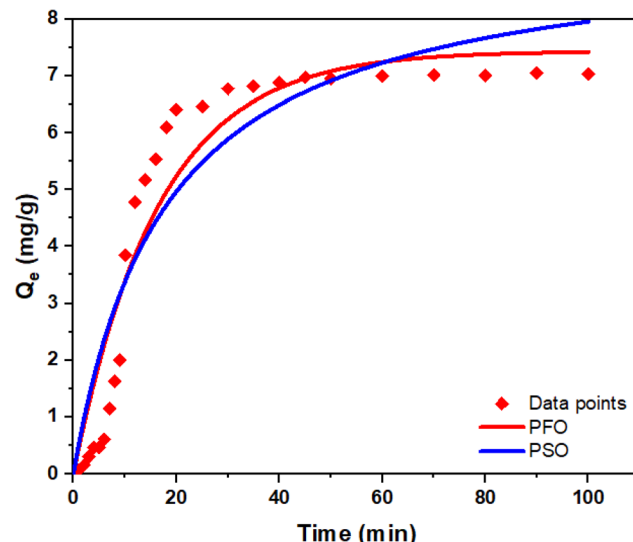
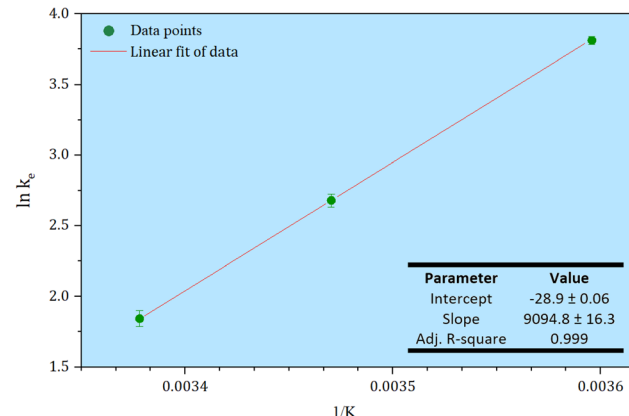
Fig. 8 Kinetic profiles at pH 7.5 and 23 °C for the coagulation-like removal of arsenic at pH 7.5 with both  $\text{H}_2\text{AsO}_4^-$  and  $\text{HAsO}_4^{2-}$  species present. The fitted lines correspond to the best-fit results for the PFO and PSO kinetic models.

Fig. 10 A van't Hoff plot for estimation of the thermodynamic parameters of the arsenic adsorption process.

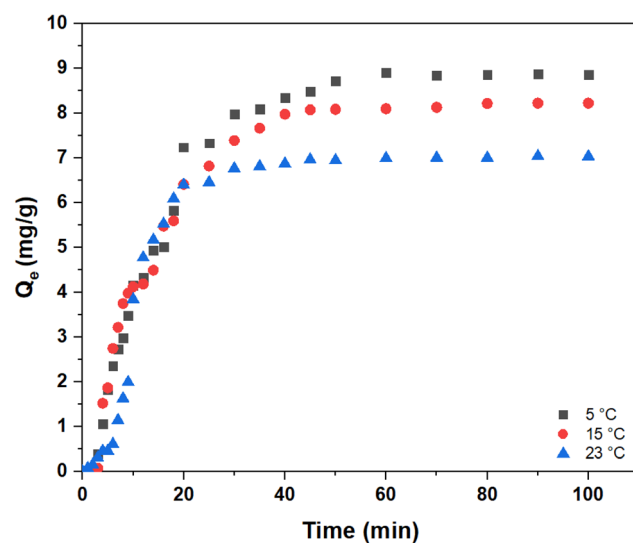


Fig. 9 Evaluation of the thermodynamic parameters of the arsenic adsorption process through kinetic experiments at 5 °C, 15 °C and 23 °C at pH 7.5.

80 kJ mol<sup>-1</sup>. The obtained value is slightly below this threshold ( $-75 \text{ kJ mol}^{-1}$ ) that concurs with a physisorption process.<sup>64</sup>

Interestingly, the negative  $\Delta S^\circ$  value would indicate that the adsorption process contributes to reduced disorder overall. It is

Table 5 Thermodynamic parameters for the arsenic removal with Chi-Py at pH 7.5

Temperature (K)	$\Delta G^\circ$ (kJ mol <sup>-1</sup> )	$\Delta H^\circ$ (kJ mol <sup>-1</sup> )	$\Delta S^\circ$ (J K mol <sup>-1</sup> )
296.1	-4.7	-75.6	-233.4
288.1	-6.6		
278.1	-9.0		

therefore posited, that during the adsorption process, the low hydration energy and subsequent dehydration and association process outweighs any potentially increased disorder through liberated solvent from the solvated anions. In summary, although  $\Delta S^\circ$  does not favour a spontaneous process, the exothermic nature of the association process results in favourable adsorption overall. The adsorption process becomes non-spontaneous at a temperature above *ca.* 42 °C.

## 4. Conclusion

In this study, a pyridinium-modified insoluble chitosan-derivative (Chi-Py) was prepared through an adapted solid-phase synthesis that employs DMSO as the solvent for use in a coagulation-flocculation-based methodology for facile integration within existing water treatment processes. The characterization was performed *via* spectroscopy (FT-IR, <sup>13</sup>C solids NMR, XPS) and TGA. The modified biopolymer was shown to contain both pyridinium chloride (*ca.* 30%) and di-nitro-containing moieties (*ca.* 7%) that are covalently bound and remain grafted to the biopolymer structure even after exposure to aqueous media. The coagulation study unveiled that, an arsenic concentration at



5 mg L<sup>-1</sup> and at 23 °C, resulted in 70% removal at a Chi-Py dosage of 150 mg L<sup>-1</sup>, whereas maximum removal of 76% occurred at a dosage of 300 mg L<sup>-1</sup>. By contrast, chitosan displayed a 4% removal under the same conditions, whereas FeCl<sub>3</sub> reached 73% removal, while the binary (FeCl<sub>3</sub> + chitosan) system only reached a 69% arsenic removal. The thermodynamics of arsenic removal via Chi-Py are listed:  $\Delta H^\circ = -75.6$  kJ mol<sup>-1</sup>,  $\Delta S^\circ = -233.4$  J K<sup>-1</sup> mol<sup>-1</sup> and  $\Delta G^\circ = -4.7$  kJ mol<sup>-1</sup> at 23 °C with a kinetic adsorption profile described by the PFO model. Furthermore, the removal efficiency increased to 96% at 5 °C (cf. Table S1; ESI<sup>†</sup>). The use of Chi-Py obviates greater dosages (gram per L to decagram per L) noted for conventional adsorbents. In contrast to common coagulants, such as FeCl<sub>3</sub>, that require a far lower dosage (at acidic conditions), where a small error in concentration can result in catastrophic loss of its removal performance, Chi-Py can be used across a broader dosage range (at pH > pH<sub>pzc</sub>) without incurring detrimental loss in the removal efficiency.

This study employed a modified chitosan-based adsorbent with pyridinium moiety for effective arsenate removal at pH 7.5 (unlike pristine chitosan) via a coagulation-based compatible process that is commonly used in WTPs. Future research hereby can be divided in two distinct directions, where reusability and improved separation can be achieved (below 10 µg L<sup>-1</sup> for arsenic), and the favourable sustainability of such materials can be studied for the treatment of environmental water samples.

## Author contributions

D. J. V.-G.: writing, editing, experimental & data analysis; B. G. K. S.: writing, conceptualisation & materials preparation/characterization, editing; L. D. W.: funding acquisition, writing – review & editing, supervision and funding.

## Conflicts of interest

The authors declare that they have no known competing financial interests or personal relationships that could have appeared to influence the work reported in this research.

## Acknowledgements

LDW gratefully acknowledges the funding provided by the Government of Canada through the Natural Sciences and Engineering Research Council of Canada (Discovery Grant Number: RGPIN 04315-2021). The Saskatchewan Structural Science Centre (SSSC) is acknowledged for providing facilities to conduct this research. The authors wish to make a land acknowledgement that this work was carried out in Treaty 6 Territory and the Homeland of the Métis. As such, we pay our respect to the First Nations and Métis ancestors of this place and reaffirm our relationship with one another.

## References

- 1 J.-Y. Chung, S.-D. Yu and Y.-S. Hong, *J. Prev. Med. Public Health*, 2014, **47**, 253–257.
- 2 G. V. Sousa, V. L. G. Teles, E. G. Pereira, L. V. Modolo and L. M. Costa, *J. Hazard. Mater.*, 2021, **123**565.
- 3 Z. Babazad, F. Kaveh, M. Ebadi, R. Z. Mehrabian and M. H. Juibari, *Heliyon*, 2021, **7**, e06631.
- 4 WHO, *Guidelines for Drinking-Water Quality Fourth Edition incorporating the first and second addends*, <https://apps.who.int/iris/rest/bitstreams/1414381/retrieve>.
- 5 A. Shah, A. Arjunan, A. Baroutaji and J. Zakharova, *Water Sci. Eng.*, DOI: [10.1016/j.wse.2023.04.003](https://doi.org/10.1016/j.wse.2023.04.003), in press.
- 6 S. Wang and C. N. Mulligan, *Sci. Total Environ.*, 2006, **366**, 701–721.
- 7 B. C. Astles, J. Chételat, M. J. Palmer and J. C. Vermaire, *PLoS One*, 2022, **17**, e0279412.
- 8 M. S. Reid, K. S. Hoy, J. R. M. Schofield, J. S. Uppal, Y. Lin, X. Lu, H. Peng and X. C. Le, *TrAC, Trends Anal. Chem.*, 2020, **123**, 115770.
- 9 Z. Zhang, J. Li, C. Sun, T. F. Marhaba, W. Zhang and Y. Zhang, *Water, Air, Soil Pollut.*, 2016, **227**, 309.
- 10 T. A. Kurniawan, W. Lo, X. Liang, H. H. Goh, M. H. D. Othman, K.-K. Chong and K. W. Chew, *Sep. Purif. Technol.*, 2023, **314**, 123474.
- 11 R. S. Neisan, N. M. C. Saady, C. Bazan, S. Zendehboudi, A. Al-nayili, B. Abbassi and P. Chatterjee, *Clean Technol.*, 2023, **5**, 352–402.
- 12 I. Issahaku, I. K. Tetteh and A. Y. Tetteh, *Environ. Adv.*, 2023, **11**, 100351.
- 13 H. Zeng, M. Arashiro and D. E. Giammar, *Water Res.*, 2008, **42**, 4629–4636.
- 14 Y. John, V. E. David and D. Mmereki, *Int. J. Chem. Eng.*, 2018, **2018**, 1–21.
- 15 A. Benhamou, J. P. Basly, M. Baudu, Z. Derriche and R. Hamacha, *J. Colloid Interface Sci.*, 2013, **404**, 135–139.
- 16 S. Rawat, M. Chaudhary and A. Maiti, *J. Environ. Chem. Eng.*, 2023, **11**, 109431.
- 17 M. T. Motloung, S. I. Magagula, A. Kaleni, T. S. Sikhosana, K. Lebelo and M. J. Mochane, *Water*, 2023, **15**, 793.
- 18 D. J. Venegas-García and L. D. Wilson, *Materials*, 2022, **15**, 8691.
- 19 S. Ahmed and S. Ikram, *Chitosan*, John Wiley & Sons, Inc., Hoboken, NJ, USA, 2017.
- 20 M. Eddy, B. Tbib and K. EL-Hami, *Heliyon*, 2020, **6**, e03486.
- 21 K. C. M. Kwok, L. F. Koong, T. Al Ansari and G. McKay, *Environ. Sci. Pollut. Res.*, 2018, **25**, 14734–14742.
- 22 R. El Kaim Billah, M. Aminul Islam, H. Lgaz, E. C. Lima, Y. Abdellaoui, Y. Rakhlila, O. Goudali, H. Majdoubi, A. A. Alrashdi, M. Agunaou and A. Soufiane, *Arabian J. Chem.*, 2022, **15**, 104123.
- 23 H. K. Agbovi and L. D. Wilson, in *Natural Polymers-Based Green Adsorbents for Water Treatment*, Elsevier, 2021, pp. 1–51.
- 24 M. M. Hassan, M. H. Mohamed, I. A. Udoetok, B. G. K. Steiger and L. D. Wilson, *Polymers*, 2020, **12**, 1502.
- 25 Q. Z. Wang, X. G. Chen, N. Liu, S. X. Wang, C. S. Liu, X. H. Meng and C. G. Liu, *Carbohydr. Polym.*, 2006, **65**, 194–201.
- 26 S. Jiang, X. Wu, S. Du, Q. Wang and D. Han, *Water*, 2022, **14**, 2813.



27 A. R. Karbassi, M. Heidari, A. R. Vaezi, A. R. V. Samani, M. Fakhraee and F. Heidari, *Environ. Earth Sci.*, 2014, **72**, 457–465.

28 R. E. K. Billah, Z. Azoubi, E. A. López-Maldonado, H. Majdoubi, H. Lgaz, E. C. Lima, A. Shekhawat, Y. Tamraoui, M. Agunaou, A. Soufiane and R. Jugade, *ACS Omega*, 2023, **8**, 10051–10061.

29 L. Chen, J. Tang, S. Wu, S. Wang and Z. Ren, *Carbohydr. Polym.*, 2022, **286**, 119307.

30 J.-Z. Guo, H. Xu, L. Chen and B. Li, *Bioresour. Technol.*, 2022, **365**, 128112.

31 F. Gonçalves and R. Freitas, *J. Braz. Chem. Soc.*, 2019, **30**(11), 2318–2323.

32 M. Eda, M. J. Kurth and M. H. Nantz, *J. Org. Chem.*, 2000, **65**, 5131–5135.

33 S. Zhao, X. Xu, L. Zheng and H. Liu, *Ultrason. Sonochem.*, 2010, **17**, 685–689.

34 L. N. Pincus, H. E. Rudel, P. V. Petrović, S. Gupta, P. Westerhoff, C. L. Muhich and J. B. Zimmerman, *Environ. Sci. Technol.*, 2020, **54**, 9769–9790.

35 P. Ścigalski and P. Kosobucki, *Molecules*, 2020, **25**, 4869.

36 N. Wang, N. Wang, L. Tan, R. Zhang, Q. Zhao and H. Wang, *Sci. Total Environ.*, 2020, **726**, 138541.

37 B. R. C. Vieira, A. M. A. Pintor, R. A. R. Boaventura, C. M. S. Botelho and S. C. R. Santos, *J. Environ. Manage.*, 2017, **192**, 224–233.

38 A. Maria, E. Mayasari, U. Irawati and Zulfikurrahman, *IOP Conf. Ser.: Mater. Sci. Eng.*, 2020, **980**, 012077.

39 J. Ge, B. Guha, L. Lippincott, S. Cach, J. Wei, T. L. Su and X. Meng, *Sci. Total Environ.*, 2020, **725**, 138351.

40 C. C. Osuna-Martínez, M. A. Armienta, M. E. Bergés-Tiznado and F. Páez-Osuna, *Sci. Total Environ.*, 2021, **752**.

41 F. Hesami, B. Bina, A. Ebrahimi and M. Amin, *Int. J. Environ. Health Eng.*, 2013, **2**, 17.

42 B. S. Rathi and P. S. Kumar, *J. Hazard. Mater.*, 2021, **418**, 126299.

43 N. Fairley, V. Fernandez, M. Richard-Plouet, C. Guillot-Deudon, J. Walton, E. Smith, D. Flahaut, M. Greiner, M. Biesinger, S. Tougaard, D. Morgan and J. Baltrusaitis, *Appl. Surf. Sci. Adv.*, 2021, **5**, 100112.

44 N. K. Ibnul and C. P. Tripp, *Talanta*, 2021, **225**, 122023.

45 T. Okazaki, H. Kuramitz, N. Hata, S. Taguchi, K. Murai and K. Okauchi, *Anal. Methods*, 2015, **7**, 2794–2799.

46 D. J. Venegas-García and L. D. Wilson, *Materials*, 2023, **16**, 655.

47 H. Saito, R. Tabeta and K. Ogawa, *Macromolecules*, 1987, **20**, 2424–2430.

48 J. Wang and S. Zhuang, *J. Cleaner Prod.*, 2022, **355**, 131825.

49 J.-Z. Guo, H. Xu, L. Chen and B. Li, *Bioresour. Technol.*, 2022, **365**, 128112.

50 T. S. Jo, J. J. Koh, H. Han and P. K. Bhowmik, *Mater. Chem. Phys.*, 2013, **139**, 901–910.

51 K. Wieszczycka, K. Filipowiak, A. Lewandowska, A. Marcinkowska and M. Nowicki, *Molecules*, 2022, **27**, 1723.

52 M. Katcka and T. Urbanski, *Bull. Acad. Pol. Sci.*, 1964, **12**, 615–621.

53 N. Johar, I. Ahmad and A. Dufresne, *Ind. Crops Prod.*, 2012, **37**, 93–99.

54 Y. A. Anisimov, D. E. Cree and L. D. Wilson, *J. Compos. Sci.*, 2020, **4**, 18.

55 C. Peniche-Covas, W. Argüelles-Monal and J. San Román, *Polym. Degrad. Stab.*, 1993, **39**, 21–28.

56 N. Achalhi, Y. El Ouardi, R. El Yousfi, M. Lamsayah, S. El Barkany, K. Laatikainen and A. El Idrissi, *Cellulose*, 2023, **30**, 1483–1502.

57 F. L. Bernard, R. B. Duczinski, M. F. Rojas, M. C. C. Fialho, L. Á. Carreño, V. V. Chaban, F. D. Vecchia and S. Einloft, *Fuel*, 2018, **211**, 76–86.

58 J. F. Moulder and J. Chastain, *Handbook of X-Ray Photoelectron Spectroscopy: A Reference Book of Standard Spectra for Identification and Interpretation of XPS Data*, Physical Electronics Division, Perkin-Elmer Corporation, 1992.

59 C. Chenzhong, *J. Chem. Educ.*, 1993, **70**(1), 25.

60 M. Mohamed and L. Wilson, *Nanomaterials*, 2015, **5**, 969–980.

61 H. K. Agbovi and L. D. Wilson, *Carbohydr. Polym.*, 2018, **189**, 360–370.

62 B. S. Yadav and S. Dasgupta, *Inorg. Chem. Commun.*, 2022, **137**, 109203.

63 P. E. Ohale, C. E. Onu, N. J. Ohale and S. N. Oba, *Chem. Eng. J. Adv.*, 2020, **4**, 100036.

64 T. A. Saleh, *Interface Science and Technology*, 2022, vol. 34, pp. 39–64.

